A&A manuscript no.
(will be inserted by hand later)

Your thesaurus codes are:
03(11.01.2; 11.19.1; 11.19.3; 11.19.5

ASTRONOMY AND ASTROPHYSICS
August 9, 1999

Starbursts in active galaxy nuclei: observational constraints from IR stellar absorption lines ⋆

E. Oliva[1], L. Origlia[2], R. Maiolino[1], and A.F.M. Moorwood[3]

[1] Osservatorio di Arcetri, Largo E. Fermi 5, I-50125 Firenze, Italy
[2] Osservatorio Astronomico di Bologna, Via Ranzani 1, I–40127 Bologna, Italy
[3] European Southern Observatory, Karl Schwarzschild Str. 2, D-85478 Garching, Germany

Received 13 April 1999/ Accepted ...

Abstract. High quality infrared spectra of active galaxies including the stellar absorption features of Si at 1.59 μm, CO(6,3) at 1.62 μm, and CO(2,0) at 2.29 μm are used to measure the stellar mass to light ratio at 1.65 μm ($M/L_{\rm H}$) and investigate the occurrence of circum–nuclear starbursts. We find that old and powerful starbursts are relatively common in obscured AGNs (5 objects out of 13) while absent in genuine Seyfert 1's (0 objects out of 8).

The data are also used to derive the non–stellar continuum which is very red and compatible with emission from warm ($\simeq$1000 K) dust even in bare Sy1's, thus indicating that the near IR nuclear continuum is reprocessed radiation. Hot dust ($\simeq$800 K) emission is also detected in a few obscured AGNs, including the Seyfert 2 prototype NGC1068. The observed non–stellar flux is too high to be accounted for by scattered light and therefore indicates that the material obscuring the AGN must have a quite small ($\lesssim$1 pc) projected size.

Key words: Galaxies: active; Galaxies: starburst; Galaxies: Seyfert; Galaxies: stellar content

1. Introduction

Starburst events may recurrently occur in the central region of galaxies, over-imposed to an old, quiescent stellar population such as that found in normal galaxies. Estimating the starburst parameters – i.e. their actual age, duration, temporal and spatial evolution, the shape of the initial mass function etc. – is a very difficult and controversial task even in the "cleanest" and best studied objects. In Seyfert galaxies the situation is further complicated by the presence of the active nucleus which could out-shine and hide the emission from the starburst at most wavelengths. Although some evidence of circum–nuclear starbursts has been occasionally reported in a few type 2 Seyferts, it is not yet clear if such events are common or just incidentally related to the AGN (see e.g. the recent review by Moorwood 1996 and references therein).

Absorption features in near infrared spectra of galaxies can be used to study the cool stellar population whose physical properties mainly depend on age and metallicity. In a starburst, red supergiant and intermediate mass AGB stars dominate the IR stellar light from $\sim 10^7$ up to a few $\times 10^9$ yr while in old stellar systems the emission is dominated by low mass red giants evolving on the RGB. In a series of previous papers (Origlia et al. 1993, hereafter OMO93, Origlia et al. 1997, Oliva & Origlia 1998) we investigated the behaviour of a carefully selected set of stellar absorption features – namely Si 1.59 μm, CO(6,3) 1.62 μm and CO(2,0) 2.29 μm – with stellar parameters such as temperature, gravity, microturbulence velocity and chemical composition. We found, in particular, that the equivalent width of the CO(6,3) second overtone provides a powerful tool to measure the metallicity of stellar systems.

In Oliva et al. (1995, hereafter Paper 1) we applied our IR diagnostics to a limited sample of normal and active galaxies and used the velocity dispersion of the stellar absorption features to estimate the dynamical mass and hence the mass to light ratio of the dominant stellar population. This provided evidence for starburst events in several type 2, but not in type 1 Seyferts. This paper is a follow–up of Paper 1 including an enlarged sample of Seyferts. The data are presented in Sect. 2 and the results are discussed in Sect. 3. In Sect. 4 we draw our conclusions.

2. Observations and data reduction

The spectra were collected in March 1995 at the ESO-NTT telescope using the IRSPEC infrared spectrometer (Moorwood et al. 1991, Gredel & Weilenmann 1992). Instrument setup and observational procedures were as in Paper 1. Spectra were taken using a slit width of 4.4″ or 2 pixels which yields a resolving power of $R \simeq$1600 and 2500 at 1.6 and 2.3 μm, respectively. Each object was observed with the grating set at 1.59, 1.62 and 2.29 μm (rest wavelengths) to include the stellar absorption features of

Send offprint requests to: E. Oliva
⋆ Based on observations collected at the European Southern Observatory, La Silla, Chile.

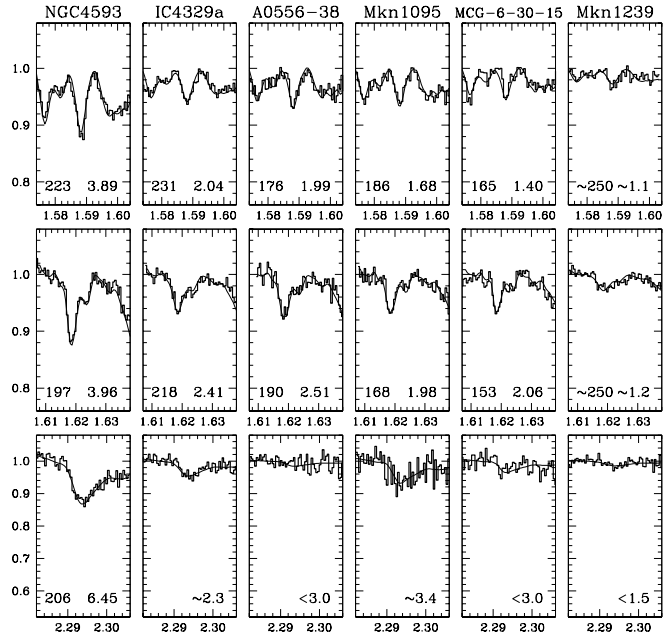

Fig. 1. Normalized spectra of type 1 Seyferts centered at the positions of the stellar absorption features of Si 1.59 μm (top panels), CO(6,3) 1.62 μm (central panels) and CO(2,0) 2.29 μm (bottom panels). Wavelengths are in the rest frame and the thin lines show the results of the spectral fit used to determine equivalent widths and velocity dispersions which are listed in Table 1.

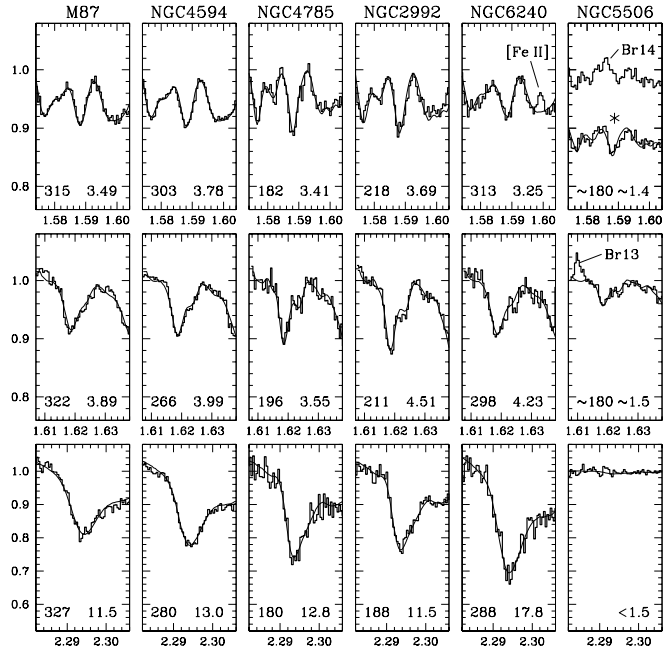

Fig. 2. Same as Fig. 1 for obscured AGNs. The top right panel also includes the spectrum of NGC5506 corrected for the Br14 hydrogen emission line which fills in the Si 1.59 feature. See the 2^{nd} paragraph of Sect. 3 where we also discuss the nebular line of [FeII] at 1.5995 μm which is visible in the spectrum of NGC6240.

interest. Each 2D spectrum consisted of several ABBA cycles (A–object, B–sky or, for compact sources, object moved $\simeq$30″ along the slit) each exposure being the mean of two 60 second frames. Total integration time per object varied between 1 and 4 hours, depending on the brightness of the source. Data were spectroscopically calibrated (i.e. corrected for instrumental and atmospheric transmission) using spectra of O5/O6 main sequence stars taken at the same grating positions as the objects. Absolute fluxes were derived from observations of photometric standard stars. The 1D spectra were extracted from the central 3 rows of the array. Data reduction was performed using the IRSPEC context in MIDAS the standard ESO reduction package. More details can be found in Oliva & Origlia 1992, Paper 1 and in the MIDAS manual.

Velocity broadening (σ=FWHM/2.35) and equivalent width of the stellar absorption features were determined using the spectral fitting procedure described in Paper 1. This best–fits the data using broadened stellar spectra taken with the same instrument and also includes a free parameter representing a featureless non–stellar continuum diluting the features. More details can be found in Sect. 2.1 of Paper 1.

3. Results and discussion

The normalized spectra are displayed in Figs. 1, 2 together with the fitted profiles. Continuum fluxes are listed in Table 1 together with the velocity dispersions and equivalent widths of the stellar features derived from the spectral fitting. As in Paper 1, the scatter between the velocity dispersions of the various features in each object indicates that the errors should not exceed $\pm$20 km/s (equivalent to about half a pixel). Typical errors on equivalent widths are $\pm$0.3 Å for Si and CO(6,3) and $\pm$0.6 Å for CO(2,0), these are mainly determined by the accuracy of continuum positioning and by the correction for velocity broadening described in Sect. 2.1 of Paper 1.

Spectral fitting was particularly difficult in the case of NGC5506, a Sy2 galaxy with unusually strong hydrogen emission lines such as Br13 (1.6109 μm), which is visible on the blue side of CO(6,3), and Br14 (1.5880 μm), which fills in the Si 1.59 feature (see the top right panel of Fig. 2). To recover the stellar absorption feature at 1.59 μm we took the observed emission profile of Br13 and added it in absorption at the position of Br14 after correction for the intrinsic Br13/Br14=1.25 ratio. The resulting spectrum is also displayed in Fig. 2 (marked by an asterisk) and its shape is compatible with $\sigma \simeq 180$ km/s, i.e. the velocity dispersion derived from CO(6,3). The only other object displaying nebular lines is NGC6240, an interacting system with extremely strong [FeII] 1.644 and H_2 2.121 μm emission lines (e.g. van der Werf et al. 1993). The satellite line of [FeII] at 1.5995 μm is clearly detected in our spectra (see Fig. 2) and was therefore excluded by the

Table 1. Observed parameters

Object	Velocity dispersions[(1)]			Equivalent widths[(2)]			Fluxes[(3)]	
	$\sigma(1.59)$	$\sigma(1.62)$	$\sigma(2.29)$	$W_\lambda(1.59)$	$W_\lambda(1.62)$	$W_\lambda(2.29)$	$F_{-11}(1.62)$	$F_{-11}(2.29)$
Seyfert 1's								
NGC 4593	223	197	206	3.9	4.0	6.5	5.7	3.3
IC 4329a	231	218	—	2.0	2.4	∼2	7.6	6.6
Mkn 1095	186	168	—	1.7	2.0	∼3	2.4	1.8
Mkn 1239[a]	∼250	∼250	—	∼1.1	∼1.2	<1	5.3	5.5
A 0556-38	176	190	—	2.0	2.5	<3	2.6	2.5
MCG-6-30-15	165	153	—	1.4	2.1	<3	4.4	3.5
Obscured AGNs[b]								
NGC 2992	218	211	188	3.7	4.5	11.5	5.8	2.7
NGC 4594[c]	303	266	281	3.8	4.0	13.0	32.	11.
NGC 4785	182	196	180	3.4	3.6	12.8	2.8	1.1
NGC 5506[d]	∼180	∼180	—	∼1.4	∼1.5	<1.5	6.5	8.8
NGC 6240[e]	313	298	288	3.3	4.2	17.8	4.0	2.3
M 87[f]	315	322	327	3.5	3.9	11.5	11.	3.8

(1) Velocity dispersions (km/s) of the stellar absorption lines Si 1.59 μm, CO(6,3) 1.62 μm, CO(2,0) 2.29 μm. Typical errors are ±20 km/s.
(2) Equivalent widths (Å) of above stellar lines. Typical errors are 0.3 Å for $W_\lambda(1.59)$, $W_\lambda(1.62)$ and 0.6 Å for $W_\lambda(2.29)$.
(3) Observed continuum flux, units of 10^{-11} erg cm^{-2} s^{-1} μm^{-1}.
[a] Continuum of Mkn 1239 is dominated by non–stellar emission, stellar features are shallow (see Fig. 1).
[b] Objects with an obscured active nucleus, classified from optical and/or X–ray spectra (see also Sect. 3.4)
[c] Optical stellar lines yield σ=256 km/s (Whitmore et al. 1985).
[d] Non-stellar continuum and hydrogen emission lines are both strong in NGC 5506 (see Fig. 2 and Sects. 3, 3.4.2).
[e] Infrared spectra of CO(2,0) by Lester & Gaffney (1994), Doyon et al. (1994) and Shier et al. (1996) yield $\sigma(2.29)$=350 km/s. This galaxy is also discussed in Sect. 3.4.3
[f] Radio galaxy, optical stellar lines yield σ=335 km/s (Whitmore et al. 1985).

spectral fitting. The line intensity is $\simeq 5\times10^{-15}$ erg cm^{-2} s^{-1} or about 3% of [FeII] 1.644 μm. This ratio indicates an electron density $\lesssim 10^3$ cm^{-3} (see Fig. 7 of Oliva et al. 1990).

3.1. Non–stellar continuum emission

The contribution of non–stellar emission to the observed continuum flux at 1.6 μm can be estimated using the $W_\lambda(1.62)$ vs. $W_\lambda(1.62)/W_\lambda(1.59)$ plot of Fig. 3.
The method relies on observations of stars and stellar clusters showing that there is a limited range of $W_\lambda(1.62)$ for a given $W_\lambda(1.62)/W_\lambda(1.59)$ ratio, and both quantities increase going to cool stars (OMO93). Warm stars (e.g. low metallicity globular clusters) have shallow CO(6,3) and relatively strong Si 1.59 and therefore lie at the bottom left of the diagram of Fig. 3. Going to lower temperatures (e.g. higher metallicity globular clusters) the strength of CO(6,3) increases much more rapidly than Si 1.59 and the point moves toward the upper right of the diagram. Objects with diluted stellar features lie below the locus occupied by stars and star clusters because they have a shallower CO(6,3) index, while $W_\lambda(1.62)/W_\lambda(1.59)$ is not significantly affected by dilution since the two features lie close in wavelength. The fraction of non–stellar continuum is simply given by the vertical displacement of the point in the diagram.

The dilution at 2.29 μm is determined in a similar way from the diagram in Fig. 4 where objects with significant non–stellar continua lie on the right hand side. The only complication is that one first needs to correct $W_\lambda(1.62)$ for dilution before determining the non–stellar fraction from the horizontal displacement in the diagram (see also Fig. 2b of Paper 1).

The effect of non–stellar emission is much more evident at the longer wavelengths where the CO(2,0) feature is weak or virtually absent in all Sy1 spectra (see Fig. 1 and Fig. 1c of Paper 1). Diluted features are less common in type 2 Seyferts, remarkable exceptions being NGC1068 (see OMO93) and NGC5506 (see Fig. 2) whose 2.29 μm spectra are basically featureless and therefore dominated by non–stellar radiation.

The stellar features around 1.6 μm are much less diluted and clearly visible in all but one object (Mkn1239). This implies that the diluting continuum is very red and its colour temperature (second last column of Table 2) is compatible with emission by relatively hot dust (≃1000 K) even in bare Sy1's such as NGC3783 and IC4329a. We do not therefore confirm the results of Kotilainen et al.

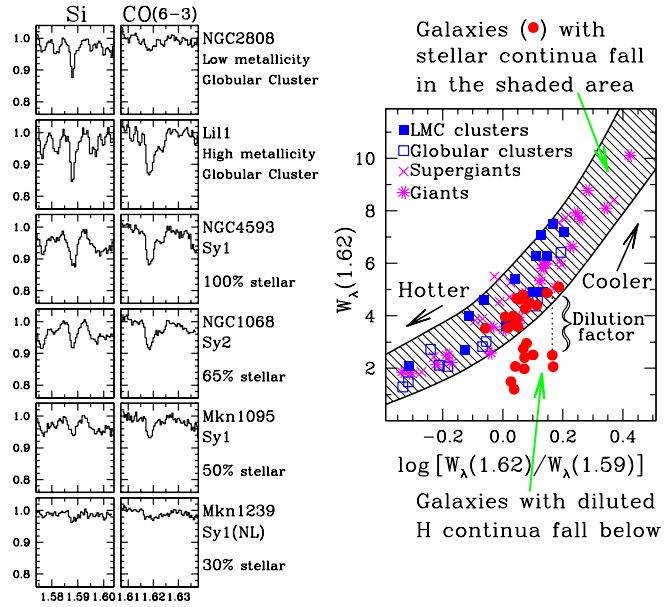

Fig. 3. The right hand panel shows the $W_\lambda(1.62)$ vs. $W_\lambda(1.62)/W_\lambda(1.59)$ diagram used to estimate the non–stellar continuum emission at 1.62 μm. Measurements of objects dominated by stellar light are marked and normalized spectra of representative objects are shown in the left hand panels. Galaxies with diluted stellar continua fall below the dashed line, see Sect. 3.1 for details.

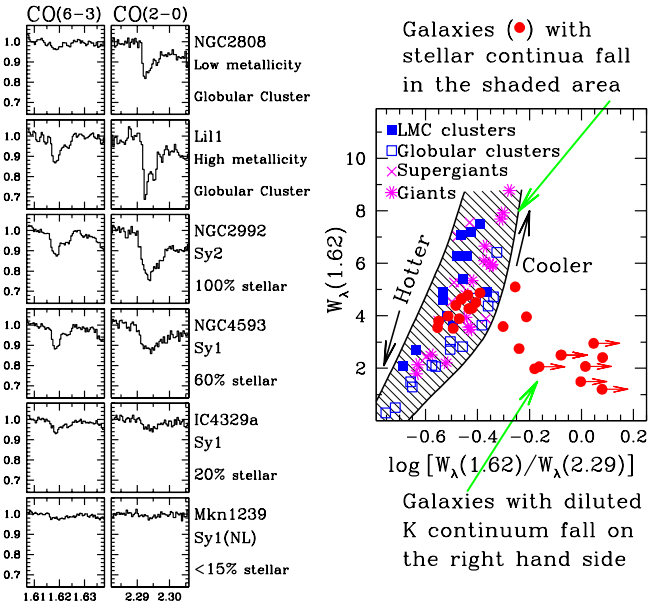

Fig. 4. Right hand panel: $W_\lambda(1.62)$ vs. $W_\lambda(1.62)/W_\lambda(2.29)$ diagram used to estimate the non–stellar continuum emission at 2.29 μm. Measurements of objects dominated by stellar light are marked and normalized spectra of representative objects are shown in the left hand panels. Galaxies with diluted stellar continua fall to the right hand side of the dashed region, see Sect. 3.1 for details.

(1992) who, based on decomposition modelling of near IR images, claim very flat nuclear continua in many Seyferts including several of those in our sample (see 7^{th} column of Table 2).

The above results indicate that the nuclear continuum at 1.6–2.3 μm is due to reprocessed radiation, i.e. emission from dusty clouds heated by AGN ultraviolet continuum and lying at a distance (e.g. Barvainis 1987)

$$R = 0.8 \left(\frac{L_{UV}}{10^{11}\,L_\odot}\right)^{1/2} \left(\frac{T_{dust}}{1000\,\mathrm{K}}\right)^{-2.8} \quad \mathrm{pc} \qquad (1)$$

where L_{UV} is the AGN luminosity in the UV and T_{dust} is the dust equilibrium temperature.

Interestingly, the dust continua of Sy2's are systematically cooler than in Sy1's, but the dust temperatures found in the type 2 Seyferts NGC5506 and NGC1068 are quite high ($\simeq$800 K) and only $\simeq$200 K cooler than those found in Sy1's. This implies that regions quite close ($\simeq$1 pc) to the nucleus are directly visible or, alternatively, that the non–stellar continuum seen in these objects is scattered radiation. This last possibility appears unlikely on energetic grounds: the observed ratios $L_{nuc}(2.29)/L_{FIR}$ are within the range spanned by Sy1's (see last column of Table 2). More specifically, if we assume that the intrinsic hot–dust spectrum of NGC1068 is the same (in luminosity and colour) to that of A0556-38, the efficiency of the scattering "mirror" must be 6%. Adopting other Sy1 templates yields more prohibitive values, e.g. 10% and 20% using IC4229a and NGC3783, respectively.

The distance over which the dust equilibrium temperature drops from 1000 to 800 K follows from Eq. (1) and is $\simeq$1 pc for L_{UV}=10^{11} $L_\odot$. Simple obscuration could account for the observed dust temperatures of NGC1068 only by fine–tuning of the thickness and inclination of the torus.

3.2. CO(2,0) equivalent widths and starburst activity

The strongly saturated CO(2,0) band–head is primarily sensitive to microturbulent photospheric motions (ξ) which increase at lower stellar temperatures and are larger in supergiants than giants of a given temperature (McWilliam & Lambert 1984, OMO93 and references therein). This indirect dependence on surface gravity is sometimes used to argue for/against the presence of red supergiants in galaxies. However, this index alone cannot be generally used as a starburst tracer because a given equivalent width could be equally well obtained with young stars of relatively low metallicity, or with an old and highly metallic population dominated by cool red giants. Adding measurements of other stellar features more sensitive to the stellar temperature, rather than ξ, may in principle help distinguishing between stellar luminosity classes. However, the results obtained in OMO93 and

Paper 1 indicate that equivalent widths alone do not generally provide a convenient tool to trace supergiants.

In practice, the only objects which can be directly classified as young stellar populations are those with $W_\lambda(2.29)$ significantly larger than the maximum equivalent width measured in the most metallic (i.e. coolest) old systems known. Based on available data, a safe borderline could be drawn at $W_\lambda(2.29)$=15 Å and 1 Å above the values found in bright elliptical galaxies and in Terzan 1, a highly metallic globular cluster in the bulge of our Galaxy (Origlia et al. 1997).

However, such a selection criterion is not necessarily useful for tracing red–supergiants. On the one hand, many (but not all) of the young LMC clusters display CO(2,0) indices lying well above the 15 Å borderline (see Table 1 of Oliva & Origlia 1998). On the other hand, well known starbursters often fall close or below this limit. In particular, only 1/3 of the starburst galaxies studied in Paper 1 display unmistakably strong CO(2,0) features (see Table 2 of Paper 1). Even more confusing is the case of NGC6240 which displays an extremely strong CO(2,0) feature ($\simeq$18 Å, see Table 1) but whose starburst origin has been sometimes questioned in the literature (e.g. Lester & Gaffney 1994).

3.3. Mass to light ratio and starburst activity

As already discussed in Sect. 4.2 of Paper 1, the observed velocity dispersion (σ) can be directly related to the dynamical mass of the system by assuming that the stars responsible for the IR emission are moving in a dynamically relaxed isothermal sphere whose effective diameter is larger than the projected size of the spectrometer aperture. Within these limits, the dynamical mass and the mass to light ratio ratio are simply given by

$$M = 5.6 \times 10^8 \left(\frac{\sigma}{100\,\mathrm{km/s}}\right)^2 \left(\frac{D}{10\,\mathrm{Mpc}}\right) \left(\frac{\theta_{obs}}{5''}\right) \quad M_\odot \tag{2}$$

$$M/L_\mathrm{H} = \frac{2.1}{F_{11}} \left(\frac{\sigma}{100\,\mathrm{km/s}}\right)^2 \left(\frac{D}{10\,\mathrm{Mpc}}\right)^{-1} \left(\frac{\theta_{obs}}{5''}\right) \tag{3}$$

where θ_{obs} is the spectrometer aperture, D is the distance to the galaxy, σ the stellar velocity dispersion and F_{11} the observed stellar flux ($\times 10^{-11}$ erg cm^{-2} s^{-1} μm^{-1}) corrected for the non–stellar (nuclear) contribution, as described in Sect. 3.1, and de–reddened adopting an intrinsic stellar colour H–K=0.2. The value of M/L_H is expressed in the conventional solar units, i.e. normalizing the stellar L_λ to $L_\odot$(H)=4.48 $\times$ 10^{32} erg s^{-1} μm^{-1}, the solar luminosity in the H band.

The available data and derived mass to light ratios are summarized in Table 3 while the distribution of M/L_H in different types of galaxies is displayed in Fig. 5 where we also include values for spirals and ellipticals from IR photometric data and optical σ's (Whitmore et al. 1985, Impey et al. 1986).

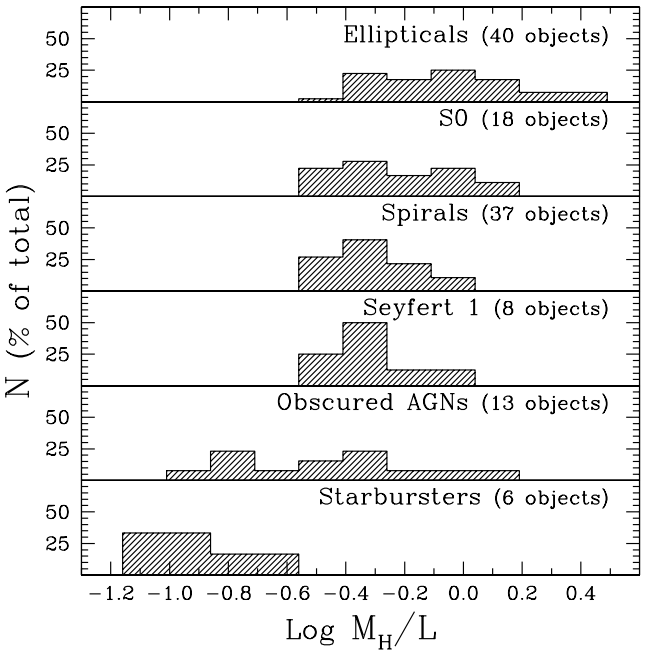

Fig. 5. Distribution of mass to light ratios inferred from the stellar flux and velocity dispersions derived from the IR spectra. Note that all the starbursters are clearly separated from normal galaxies, while the distribution of Sy1's is very similar to that of normal spirals (both have a mean value of 0.5).

All normal galaxies have mass to light ratios in the range 0.3–3 and consistent with a population of old (giant) stars plus a quiescent star formation activity (if any). The distribution of starbursters occupies only the region with M/L_H<0.25 and is clearly separated from that of normal galaxies. This demonstrate that the value of M/L_H provides an unambiguous tool to trace powerful starburst events.

The most striking result is that the distributions of Sy1's and normal spirals are virtually indistinguishable (both have a mean value of 0.51), while about half of the obscured AGNs have much lower mass to light ratios and similar to those found in genuine starbursters. This indicates that obscured AGNs have experienced starburst activity within a region of a few arcsec from the nucleus. Such an event is likely to be old ($\gtrsim$100 Myr) and extremely powerful. Old, because its associated HII regions (if any) are often not detected in hydrogen recombination lines (see Paper 1). Powerful, because the mass to light ratio is significantly decreased only if the old starburst has produced enough red supergiant/AGB stars to out-shine the background emission from the old population of RGB stars or, in practice, if the mass of gas processed into stars is at least a few % of the galaxy mass. This also implies that, sometimes in the past, the starburst was 1–2 orders of magnitude more luminous and probably out–shone the AGN (if any), i.e. the galaxy could be classified as a genuine starburster. It

Table 3. Derived mass to light ratios

Object	D[(1)]	F_*(H)[(2)]	σ[(3)]	$M/L_{\rm H}$[(4)]
Type 1 Seyferts				
NGC 1365	20	7.3	151	0.33
NGC 3783	37	3.1	152	0.43
NGC 4593	37	5.4	209	0.47
IC 4329a	64	4.3	225	0.39
Mkn 1095	130	1.1	177	0.45
Mkn 1239	78	1.5	$\sim$250[b]	$\sim$1.0
Fairall 9	186	1.0	228	0.60
MCG-6-30-15	30	1.7	159	1.08
A 0556-38	138	1.3	183	0.38
Obscured AGNs[a]				
NGC 1052	10	10.	212	0.91
NGC 1068	19	16.	160	**0.18**
NGC 2110	29	12.	268	0.44
NGC 2992	31	7.9	206	0.37
NGC 4594	15	30.	280	0.37
NGC 4785	50	3.5	187	0.43
NGC 4945	4	52.	134	**0.18**
NGC 5506	24	4.2	$\sim$180[b]	$\sim$0.7
NGC 6240	98	10.	300	**0.18**
NGC 7582	19	20.	157	**0.13**
Circinus	4	71.	168	**0.21**
A 0945-30	31	6.6	206	0.44
M 87	19	10.	321	1.10
Starbursters				
NGC 253	4	56.	109	**0.11**
NGC 1614	62	9.2	150	**0.08**
NGC 1808	10	25.	154	**0.20**
NGC 3256	35	9.3	127	**0.10**
NGC 7552	22	15.	104	**0.07**
NGC 7714	40	3.7	117	**0.19**

(1) Adopted distance (Mpc).
(2) Stellar flux at 1.65 μm [$=F_*(1.62\,\mu{\rm m})/1.06$, units of 10^{-11} erg cm^{-2} s^{-1} μm^{-1}] corrected for reddening using the extinction $A_{\rm H}$ listed in Table 2.
(3) Average dispersion velocity of stellar absorption features (km/s, see Table 1).
(4) Mass to light ratio (solar units) derived from above quantities, see Eq. (1) and Sect. 3.3. Galaxies with $M/L_{\rm H}<0.30$ are in bold type.
[a] Objects with an obscured active nucleus, classified from optical and/or X–ray spectra (see also Sect. 3.4)
[b] Stellar features are very diluted and σ is uncertain. Mkn1239 is not included in Fig. 5.

is also interesting to note that Sy1 galaxies with known circumnuclear HII regions (e.g. NGC1365) do not display unusually low $M/L_{\rm H}$ ratios, which simply indicates that the young starburst traced by the H recombination lines is relatively weak. Similarly, the young/weak starbursts traced by the rings of HII regions often found in Sy2's are not those responsible for the $M/L_{\rm H}$ ratios found here. Spectacular examples are NGC1068 and Circinus which both exhibit HII rings with radii much larger than the regions sampled in our spectra (see Neff et al. 1994, Marconi et al. 1994).

3.3.1. Possible caveats

The mass to light ratios listed in Table 3 and plotted in Fig. 5 rely on the assumption that a simple relationship between stellar velocity dispersion and dynamical mass, i.e. Eq. (2), could be used in all types of objects. Although many effects could in principle influence the σ–mass relationship (e.g. the geometry and inclination of the system), these should average out if a large enough sample of objects is considered. In particular, no systematic effect should affect the measurements of different types of Seyferts if these are really the same class of objects seen under different angles and if the orientation of the obscuring torus is not related to the inclination of the galaxy, i.e. if the AGN unification scheme is strictly correct. The only observational bias which could introduce a systematic shift of the Sy1 histogram in Fig. 5 is related to the fact that half of the Sy1's in our sample are significantly more distant than the unobscured AGNs. In these objects the dynamical mass – and hence $M/L_{\rm H}$ – could be overestimated if the projected size of the spectrometer is larger than their effective radii. However, available IR images (e.g. Kotilainen et al. 1992) indicate that the stellar continuum of these galaxies is extended over many arcsec and should therefore fill the aperture of the spectrometer. A definitive confirmation could come from spectra taken with narrower slits which should yield smaller stellar fluxes ($F\propto\theta$) and similar mass to light ratios as those derived here.

3.4. Comments on individual sources

3.4.1. NGC4945

This nearby spiral is a spectacular example of the AGN–starburst dichotomy. At wavelengths shorter than 1 keV the object appears as a genuine starburster and all the observational properties, including its FIR luminosity, can be accounted for by starburst activity alone. Prior to the X–ray observations discussed below, this galaxy was usually classified as a starburster, a scheme which was also adopted in Paper 1. When looked at in the X–rays, however, the galaxy becomes the perfect example of an absorbed Seyfert 2 nucleus, i.e. powerful emission at $\gtrsim$100 keV (NGC4945 is the brightest Sy2 in the hard–X sky, Done et al. 1996) which rapidly fades at lower energies where the AGN is also revealed by a prominent Fe–K line with an equivalent width of $\simeq$1 keV. The hard X–ray luminosity and $L(100\ {\rm keV})/L(FIR)$ ratio are similar to those found in the Circinus galaxy, a nearby Sy2 whose IRAS luminosity is fully accounted for by the AGN alone (Oliva

et al. 1999). It is therefore likely that the FIR luminosity of NGC4945 is also dominated by the active nucleus.

3.4.2. NGC5506

This Seyfert 2 galaxy is the only AGN in our sample with detectable Br13, Br14 hydrogen emission lines (see Fig. 2). The optical spectrum is also characterized by prominent narrow lines over a relatively faint continuum. The equivalent width of Hα is $\simeq$400 Å, i.e. among the largest observed in Sy2's (e.g. Morris & Ward 1988) and comparable to that found in young starburst galaxies whose spectra are dominated by HII regions photoionized by massive O stars. However, the large strength of high excitation lines ([NeV], [FeVII], HeII) argue for a non–stellar ionizing continuum.

The IR continuum is dominated by emission from hot dust which strongly dilutes the absorption features even at 1.6 μm (see Fig. 2). The inferred mass to light ratio, although uncertain, is compatible with a normal (old) stellar population.

3.4.3. NGC6240

This peculiar object is an interacting system with a bolometric luminosity close to the limit of IRAS ultraluminous galaxies. A deeply hidden AGN is revealed by X–ray spectra showing a prominent FeK 6.4 KeV line and powerful continuum emission at 100 keV (Iwasawa & Comastri 1998, Iwasawa 1999, Matt 1999). The active nucleus is much less evident at longer wavelengths but its contribution to the bolometric luminosity is likely to be important because the $L(100\ \mathrm{keV})/L(FIR)$ ratio is similar to that measured in the Circinus galaxy.

Several IR spectroscopic studies exist in the literature (Doyon et al. 1994, Lester & Gaffney 1994, Shier et al. 1996) reaching contradictory conclusions on the nature of the red stellar population, i.e. young supergiants/AGB stars vs. old, low mass giants. In particular, the very large velocity dispersion and relatively high mass to light ratio have been used to argue for an old elliptical–like system (e.g. Doyon et al. 1994). However, these conclusions were drawn without correcting the stellar flux for extinction which is indeed very high, about 1 magnitude at 1.65 μm (see Table 2).

The mass to light ratio derived here is unequivocally in the starburst domain and demonstrates that the near IR emission from this massive object is still dominated by a young stellar population. It should be noted that this conclusion is still valid if the larger velocity dispersion quoted in the above papers, i.e. σ=350 km/s, is adopted.

Another peculiarity of this object is the combination of very strong CO(2,0), the deepest in our sample, and relatively shallow CO(6,3). The ratio $W_\lambda(2.29)/W_\lambda(1.62)$=4.1 is 30% larger than in starburst galaxies and young LMC clusters (see Table 1 and Fig. 5 of Oliva & Origlia 1998). The only other object with a comparably large ratio is NGC330, a well known young and metal poor cluster in the SMC. Since $W_\lambda(1.62)$ is much more sensitive to metallicity than $W_\lambda(2.29)$, this indicates that NGC6240 is a relatively metal poor system as well. Detailed modelling confirms this idea and yields a metallicity $\simeq$1/10 solar, the lowest among the galaxies in our sample (see Oliva & Origlia 1998).

4. Conclusions

Spectra of active galaxies including the stellar absorption features of Si at 1.59 μm, CO(6,3) at 1.62 μm, and CO(2,0) at 2.29 μm have been used to trace red supergiants and thus investigate the occurrence of old/exhausted circum–nuclear starbursts. We find that the commonly used CO first overtone spectroscopic/photometric index does not provide a reliable diagnostic for distinguishing red supergiants, i.e. starbursts, from metallic red giants, i.e. old stellar systems.

A much more sensitive starburst tracer is the mass to light ratio at 1.65 μm (M/L_{H}) which is derived from the observed stellar flux (de-reddened and corrected for non-stellar emission) and velocity dispersion of the stellar absorption features. All starbursters old enough to have produced red supergiants do display values of M/L_{H} at least 4 times smaller than normal elliptical/spirals.

In active galaxy nuclei, old and powerful starbursts are relatively common in obscured AGNs (5 objects out of 13) while absent in Seyfert 1's (0 objects out of 8). If confirmed on a larger sample, this result may add support to AGN evolutionary models such as those originally proposed to explain the nature of ultraluminous IRAS galaxies and their possible relationship with quasars (e.g. Sanders et al. 1988, Norman & Scoville 1988, Heckman et al. 1989). In this scenario circum–nuclear starburst and nuclear activity are both triggered by gas accreting toward the nucleus which also accounts for the obscuration of the AGN at early stages of its evolution.

Another interesting result is that the non–stellar continuum is very red and compatible with emission from hot ($\simeq$1000 K) dust even in bare Sy1's such as NGC3783 and IC4329a. Therefore, we do not confirm previous claims of much flatter nuclear spectra and find strong indication that the featureless continuum in the near IR is due to reprocessed AGN radiation in all types of Seyferts. Moreover, the nuclear non–stellar continuum of Sy2's (when detected) is only slightly cooler ($\simeq$800 K) than in Sy1's. The observed flux is too high to be accounted for by scattered light and therefore indicates that the material obscuring the AGN must have a quite small ($\lesssim$1 pc) projected size.

Acknowledgements. This work was partly supported by the Italian Ministry for University and Research (MURST) under grant Cofin98-02-32. We are grateful to the anonymous referee for his/her comments and critics which helped us to improve the quality of the paper.

References

Barvainis R., 1987, ApJ 320, 537
Done C., Madejski G.M., Smith D.A., 1996, ApJ 463, L63
Doyon R., Wells M., Wright G.S., et al., 1994, ApJ 437, L23
Gredel R., Weilenmann U., 1992, The Messenger 70, 62
Heckman T.M., Blitz L., Wilson A. S., Armus L., Miley G. K., 1989, ApJ 342, 735
Impey C.D., Wynn-Williams C.G., Becklin E.E., 1986, ApJ 309, 572
Iwasawa K., 1999, MNRAS 302, 96
Iwasawa K., Comastri A., 1998, MNRAS 297, 1219
Kotilainen J.K., Ward M.J., Boisson C., DePoy D.L., Smith M.G., 1992, MNRAS 256, 125
Lester D.F., Gaffney N.I., 1994, ApJ 431, L1
Marconi A., Moorwood A.F.M., Origlia L., Oliva E., 1994, The Messenger 78, 20
Matt G., 1999, personal communication
McWilliam A., Lambert D.L., 1984, PASP 96, 882
Moorwood A.F.M., 1996, Space Science Rev. 77, 303
Moorwood A.F.M, Moneti A., Gredel R., 1991, The Messenger 63, 77
Morris S.L., Ward M.J., 1988, MNRAS 230, 639
Neff S.G., Fanelli M.N., Roberts L.J. et al. 1994, ApJ 430, 545
Norman C., Scoville N., 1988, ApJ 332, 164
Oliva E., Origlia L., 1992, A&A 280, 536
Oliva E., Origlia L., 1998, A&A 332, 46
Oliva E., Moorwood A.F.M., Danziger I.J., 1990, A&A 240, 453
Oliva E., Origlia L., Kotilainen J.K., Moorwood A.F.M., 1995, A&A 301, 55 (Paper 1)
Oliva E., Marconi A., Moorwood A.F.M., 1999, A&A 342, 87
Origlia L., Moorwood A.F.M., Oliva E., 1993, A&A 280, 536 (OMO93)
Origlia L., Ferraro F.R., Fusi Pecci F., Oliva E., 1997, A&A 321, 859
Sanders D. B., Soifer B. T., Elias J. H., Neugebauer G., Matthews K., 1988 ApJ 328, L35
Shier L.M., Rieke M.J., Rieke G.H., 1996, ApJ 470, 222
van der Werf P., Genzel R., Krabbe A., et al., 1993, ApJ 405, 522
Whitmore B.C., McElroy D.B., Tonry J.L., 1985, ApJS 59, 1

Table 2. Stellar fluxes, reddening and non–stellar continua.

Object	Stellar[(1)]			Non–stellar[(2)]				
	$F_*(1.62)$	$F_*(2.29)$	A_H[(3)]	$F_{nuc}(1.62)$	$F_{nuc}(2.29)$	α	T_{dust}	$L_{2.29}/L_{FIR}$[(4)]
Seyfert 1's								
NGC 4593	5.7 (100%)	2.0 (60%)	0.0	<0.6	1.3	>4 (2.8)[a]	<900	0.17
IC 4329a	4.6 (60%)	1.6 (25%)	0.0	3.0	5.0	3.5 (0.7)[a]	940	1.3
Mkn 1095	1.2 (50%)	.45 (25%)	0.0	1.2	1.4	2.4	1080	0.93
Mkn 1239	1.6 (30%)	<0.6 (<10%)	0.0	3.7	4.9	2.8	1030	1.5
MCG-6-30-15	1.8 (40%)	<0.7 (<20%)	<0.3	2.6	2.9	2.3 (2.4)[a]	1100	1.3
A 0556-38	1.4 (55%)	<0.5 (<20%)	0.0	1.2	2.0	3.5	940	2.3
NGC 1365[b]	7.8 (65%)	2.9 (40%)	0.0	4.2	4.4	2.1	1130	0.01
NGC 3783[b]	3.3 (55%)	<1.2 (<20%)	0.0	2.7	4.6	3.6 (1.8)[a]	930	0.63
Fairall 9[b]	1.1 (50%)	<0.4 (<25%)	0.0	1.1	1.2	2.4 (2.3)[a]	1090	–
Obscured AGNs[c]								
NGC 2992	5.8 (100%)	2.4 (90%)	0.4	<0.6	∼0.3	>0.0		∼0.01
				∼1.5[d]	∼3[d]	∼4 (3.4)[a]	∼900	∼0.1
NGC 4594	32. (100%)	11. (100%)	0.0	<3	<1	–	–	<0.08
NGC 4785	2.8 (100%)	1.1 (100%)	0.3	<0.3	<0.1	–	–	<0.009
NGC 5506	2.6 (40%)	<1.3 (<15%)	0.6[e]	3.9	7.7	4.0 (3.5)[a]	890	0.46
NGC 6240	4.0 (100%)	2.3 (100%)	1.1	<0.4	<0.5	–	–	<0.01
M 87	11. (100%)	3.8 (100%)	0.0	<1	<0.8	–	–	<0.70
NGC 1052[b]	11. (100%)	4.0 (100%)	0.0	<1	<0.8	–	–	<0.38
NGC 1068[b]	17. (65%)	<6.6 (<20%)	<0.3	9.0	26.	5.1	780	0.07
NGC 2110[b]	7.3 (100%)	3.3 (100%)	0.6	<0.8	<0.3	–	–	<0.03
NGC 4945[b]	6.6 (100%)	6.3 (100%)	2.3	<0.7	<1.3	–	–	<0.001
NGC 7582[b]	9.5 (100%)	4.9 (70%)	0.9	<1	2.0	>4 (2.9)[a]	<900	0.02
Circinus[b]	36. (100%)	18. (100%)	0.8	<4	<4	–	–	<0.006
A 0945-30[b]	7.0 (100%)	2.5 (60%)	0.0	<0.8	1.6	>4	<900	–
Starbursters								
NGC 253[b]	18. (100%)	11. (100%)	1.3	<2	<2	–	–	<0.001
NGC 1614[b]	4.7 (100%)	2.3 (100%)	0.8	<0.5	<0.5	–	–	<0.008
NGC 1808[b]	17. (100%)	7.3 (100%)	0.5	<2	<1.5	–	–	<0.008
NGC 3256[b]	5.2 (100%)	2.5 (100%)	0.7	<0.5	<0.5	–	–	<0.003
NGC 7552[b]	8.9 (100%)	4.0 (100%)	0.6	<0.9	<0.8	–	–	<0.005
NGC 7714[b]	3.0 (100%)	1.2 (100%)	0.3	<0.3	<0.3	–	–	<0.01

(1) Stellar flux in absolute units ($\times 10^{-11}$ erg cm^{-2} s^{-1} μm^{-1}) and in percentage (in brackets) of the total observed flux, note that "100%" means ≥90% at 1.62 μm and ≥80% at 2.29 μm. These were derived using the equivalent width diagrams (Figs. 3, 4) discussed in Sect. 3.1.

(2) Non–stellar flux in absolute units ($\times 10^{-11}$ erg cm^{-2} s^{-1} μm^{-1}) and with shape parameterized in terms of a power law slope ($F_\nu \propto \nu^{-\alpha}$) and temperature of gray dust emission (T_{dust}, with $\kappa_\lambda \propto \lambda^{-1.5}$).

(3) Extinction at H (1.65 μm) assuming an intrinsic stellar colour H–K=0.2 [i.e. $F(1.62)/F(2.29)$=2.9] and a reddening curve $A_\lambda \propto \lambda^{-1.8}$, errors are ≈0.1 mag. Note that "0.0" effectively means <0.2.

(4) $L_{2.29} = \nu L_\nu(2.29)$ is the luminosity of the non–stellar component, $L(FIR)$ is the luminosity in the IRAS bands.

[a] Values in brackets are the power law slopes derived by Kotilainen et al. (1992) using imaging decomposition techniques. Note that their very flat indices for NGC3783 and IC4329a are not confirmed by our data.

[b] Data from Paper 1

[c] Objects with an obscured active nucleus, classified from optical and/or X–ray spectra (see also Sect. 3.4)

[d] The nucleus of NGC 2992 was observed in a low state. The higher fluxes are from the Feb 1988 observations of Kotilainen et al. (1992) after subtraction of the stellar fluxes derived here.

[e] Reddening in NGC 5506 from hydrogen recombination lines.